Electrochemistry **Hot Paper**

International Edition: DOI: 10.1002/anie.201707064
German Edition: DOI: 10.1002/ange.201707064

Low-Temperature Molten-Salt Production of Silicon Nanowires by the Electrochemical Reduction of $CaSiO_3$

Yifan Dong, Tyler Slade, Matthew J. Stolt, Linsen Li, Steven N. Girard, Liqiang Mai, and Song Jin**

Abstract: *Silicon is an extremely important technological material, but its current industrial production by the carbothermic reduction of SiO_2 is energy intensive and generates CO_2 emissions. Herein, we developed a more sustainable method to produce silicon nanowires (Si NWs) in bulk quantities through the direct electrochemical reduction of $CaSiO_3$, an abundant and inexpensive Si source soluble in molten salts, at a low temperature of 650 °C by using low-melting-point ternary molten salts $CaCl_2$–$MgCl_2$–NaCl, which still retains high $CaSiO_3$ solubility, and a supporting electrolyte of CaO, which facilitates the transport of O^{2-} anions, drastically improves the reaction kinetics, and enables the electrolysis at low temperatures. The Si nanowire product can be used as high-capacity Li-ion battery anode materials with excellent cycling performance. This environmentally friendly strategy for the practical production of Si at lower temperatures can be applied to other molten salt systems and is also promising for waste glass and coal ash recycling.*

Silicon is not only the foundational material for microelectronics but also a key material in many renewable energy technologies and chemical and metallurgical applications.[1] The demand for Si is increasing rapidly. For the solar energy industry alone, demand is estimated to increase 30% each year.[2] As the second most abundant element in the earth's crust, Si is naturally found in silica (SiO_2) and metal silicates, which are the primary components of rocks and sand.[3] Currently, Si is industrially produced by the carbothermic reduction of SiO_2 by coke (elemental carbon or charcoal), which requires high operating temperatures (1700 °C or higher) in an electric furnace. The net reaction is [Equation (1)]:

$$SiO_2(s) + C(s) \rightarrow Si(l) + CO_2(g) \qquad (1)$$

While this approach is scalable, it suffers from high energy consumption ($>20\,kWh\,kg^{-1}$), has poor energy efficiency ($<30\,\%$),[4] and produces significant carbon emissions directly as CO_2 and through the generation of electricity required to power high temperature furnaces.[5] Additionally, purification steps based on hydrochlorosilane through the Siemens process are needed to make high-purity Si.[6] Thus, the high cost of Si is due mainly to the large energy consumption associated with its production. Thermal reduction with reactive metals such as Mg can also reduce silica to Si,[7] but Mg comes from electrolysis as well. These factors make developing a more sustainable and energy efficient method for producing Si highly desirable.

Electrochemical reduction methods using inorganic molten salts as electrolytes have achieved great success in industrial production of aluminum (Hall–Héroult process), as well as extraction of other active metals.[8] Electrolytic Si extraction through the direct electrochemical reduction of solid silica in molten salts has also been studied. In this process, a working electrode supplies electrons to reduce the SiO_2 solid wrapped by the electrode and submerged in molten $CaCl_2$ at 850 °C via the reaction shown in Equation (2):[9]

$$SiO_2 + 4\,e^- \rightarrow Si + 2\,O^{2-} \qquad (2)$$

This approach has two major advantages over carbothermic reduction:[10] The use of molten salts significantly reduces the reaction temperature (850 vs. ca. 1700 °C), and Si is produced in a single step.[11] Furthermore, CO_2 emissions are reduced because of the lower energy consumption. However, since the electrolysis occurs at the three-phase interface between the working electrode, insulating silica solid, and molten salt, it is difficult to achieve complete reduction of the silica and the yield of Si is very low, as only the silica in contact with metal electrode is readily reduced.[12] Another issue is that the operating temperature is still too high for practical production using available compatible materials.[13] If the yield can be improved and the operating temperature can be reduced further by just a few hundred degrees, the residual heat of many industrial processes can be used to enable the practical and large scale production of Si.[14]

Herein, we overcome these limitations and develop a novel process more similar to the Hall–Héroult process to realize the low-temperature electrochemical production of Si in bulk quantities through the reduction of a soluble $CaSiO_3$ precursor using a carefully designed low-temperature ternary eutectic melt that lowers the operating temperature yet retains the solubility of $CaSiO_3$ and CaO as a supporting electrolyte that provides a higher concentration of O^{2-} ions to

---

[*] Y. Dong, T. Slade, M. J. Stolt, L. Li, Dr. S. N. Girard, Prof. S. Jin
Department of Chemistry, University of Wisconsin-Madison
1101 University Avenue, Madison, Wisconsin 53706 (USA)
E-mail: jin@chem.wisc.edu

Y. Dong, Prof. L. Mai
State Key Laboratory of Advanced Technology for Materials Synthesis and Processing, Wuhan University of Technology
122 Luoshi Road, Wuhan 430070 (China)
E-mail: mlq518@whut.edu

Dr. S. N. Girard
Department of Chemistry, University of Wisconsin-Whitewater
800 W. Main Street, Whitewater, Wisconsin 53190 (USA)

Supporting information and the ORCID identification number(s) for the author(s) of this article can be found under: https://doi.org/10.1002/anie.201707064.

© 2017 Wiley-VCH Verlag GmbH & Co. KGaA, Weinheim

improve the reaction kinetics. These advances enabled the high-yield electrolytic synthesis of Si nanowires at a low reaction temperature of 650 °C.

We carried out the electrochemical reduction in a symmetrical two-electrode setup (Figure 1) using individual graphite rods as the cathode and anode. We tried to electrochemically reduce SiO_2 powder in a $CaCl_2$ melt to produce Si at 850 °C [Equation (2)] at a constant voltage of −1.6 V following earlier reports.[4] The reaction produced a small quantity (ca. 25 mg) of micrometer-sized Si particles after 3 h (Supporting Information, Figure S1).

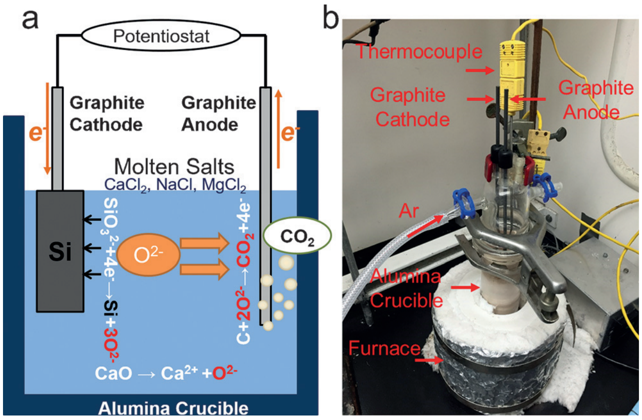

Figure 1. a) Schematic of a molten salt electrochemical cell and the various species and reactions involved. b) The working cell.

To increase the product yield, we used soluble $CaSiO_3$ instead of the sparingly soluble SiO_2 as the Si source. It was hypothesized that the higher solubility of $CaSiO_3$ in molten $CaCl_2$ could facilitate the reduction of SiO_2,[12] therefore we directly used $CaSiO_3$ as the precursor, which is an abundant and inexpensive silicate mineral.[3] The reaction preparation process and the process flow to separate the product formed on the graphite cathode from molten salts is described in detail in the Supporting Information, Materials and Methods and Figure S2. After an identical electrolysis reaction at 850 °C for 3 h at −1.6 V, the total mass of the deposited Si product from $CaSiO_3$ on the graphite rod was doubled to 55 mg (Supporting Information, Figure S3). Unlike previous reports on solid–solid electrochemical reduction of SiO_2,[9,15] in the melt, $CaSiO_3$ would dissolve to generate Ca^{2+} and SiO_3^{2-} ions [Equation (3)]:

$$CaSiO_3(s) \rightarrow Ca^{2+} + SiO_3^{2-} \qquad (3)$$

Then, on the surface of cathode, SiO_3^{2-} (including SiO_4^{4-} and $Si_xO_yCl_z^{n-}$ or other complexes; SiO_3^{2-} is used in this case as a representative example) is reduced to Si under constant influx of electrons and generates O^{2-} ions through the following reactions [Figure 1 a and Equations (4) and (5)]:

$$SiO_3^{2-} + 4\,e^- \rightarrow Si(s) + 3O^{2-} \ \text{(cathode)} \qquad (4)$$

$$C(s) + O^{2-} \rightarrow CO_2 + 4\,e^- \ \text{(anode)} \qquad (5)$$

Overall, O^{2-} anions are the limiting charge carriers in the cell and drive the electrochemical reaction from cathode to anode. Therefore, the diffusion of O^{2-} ions and the solubility of $CaSiO_3$ would be the two crucial factors that govern the electrolysis rate. In order to enhance the reaction kinetics limited by the diffusion of O^{2-} ions, we sought to increase the concentration of the dissolved O^{2-} by adding CaO as a supporting electrolyte (Figure 2 a). CaO will dissociate into Ca^{2+} and O^{2-} in the molten salt. Even though CaO is not directly involved in the electroreduction of SiO_3^{2-}, a higher concentration of CaO could increase the ionic flux of the O^{2-} ions in the melt, and thus improve the reaction kinetics. Additionally, the deposition potential of calcium is too low to be considered. Initially, 0.5 g of CaO was added to the $CaCl_2$ melt (40 g) (1.25 wt %). This electrolyte system yielded significantly more Si product from 55 to 135 mg (Figure 2 b) after 3 h of electrolysis at 850 °C. The impact of CaO is also apparent in the cyclic voltammetric (CV) curves in various $CaCl_2$ melts with or without CaO (Figure 2 g). For the $CaCl_2$ melt without CaO, two pairs of pronounced CV peaks are observed at around −1.56/1.48 V (denoted as A1/C1) and −0.35/0.25 V (donated as A2/C2). As the reaction is configured as a symmetrical two-electrode system, the anodic and cathodic peaks in each pair of CV peaks are based on the same redox reactions. The initial peaks, A1 and C1, are attributed to the reduction of the dissolved silicates to form Si [Equation (4)]. The second pair, A2 and C2, are attributed to the formation and dissolution of Ca.[16] The addition of CaO clearly significantly increased the A1/C1 peak area, while the potential difference between two peaks slightly decreased. This indicates CaO also makes the electroreduction of silicate slightly more energetically favorable. However, when the amount of CaO was increased to 1.0 g (2.50 wt %), the product yield barely increased (137 mg). The CV curve was nearly identical to that with 1.25 % CaO with only a small increase in the A2/C2 peak area. This suggests that the O^{2-} anions were likely saturated in the molten $CaCl_2$. This value is lower than the reported solubility of CaO in molten $CaCl_2$ (13 wt %) at 850 °C,[17] as the dissolved $CaSiO_3$ could decrease the solubility of CaO in the same solution. Therefore, any additional CaO would result in little change in the reaction rate. This is also confirmed by the current–time curves at a constant voltage of −1.6 V (Supporting Information, Figure S4). When 1.25 % and 2.5 % CaO were added, the current remained saturated at around −20 mA, while the reaction without CaO stabilized at a current of around −10 mA.

After we understood the importance of CaO, we tried to lower the electrolysis temperature by finding suitable eutectic molten salts with lower melting points than pure $CaCl_2$ (782 °C), while fixing the supporting electrolyte CaO at 0.5 g. Using the $CaCl_2$–NaCl eutectic system with the lowest melting point of 601 °C, the reaction temperature could be lowered to 700 °C (Table S1). However, after a 3 h of electrolysis at −1.6 V, the best product yield was significantly lower at merely 15 mg (Figure 2 d and the Supporting Information, Figure S5). We then turned to $MgCl_2$, which can also decrease the overall eutectic temperature, and has similar properties to $CaCl_2$.[17] In the $CaCl_2$–$MgCl_2$ melts, the product yield reached 60 mg at the same reaction temperature of 700 °C (Figure 2 e). We hypothe-

© 2017 Wiley-VCH Verlag GmbH & Co. KGaA, Weinheim

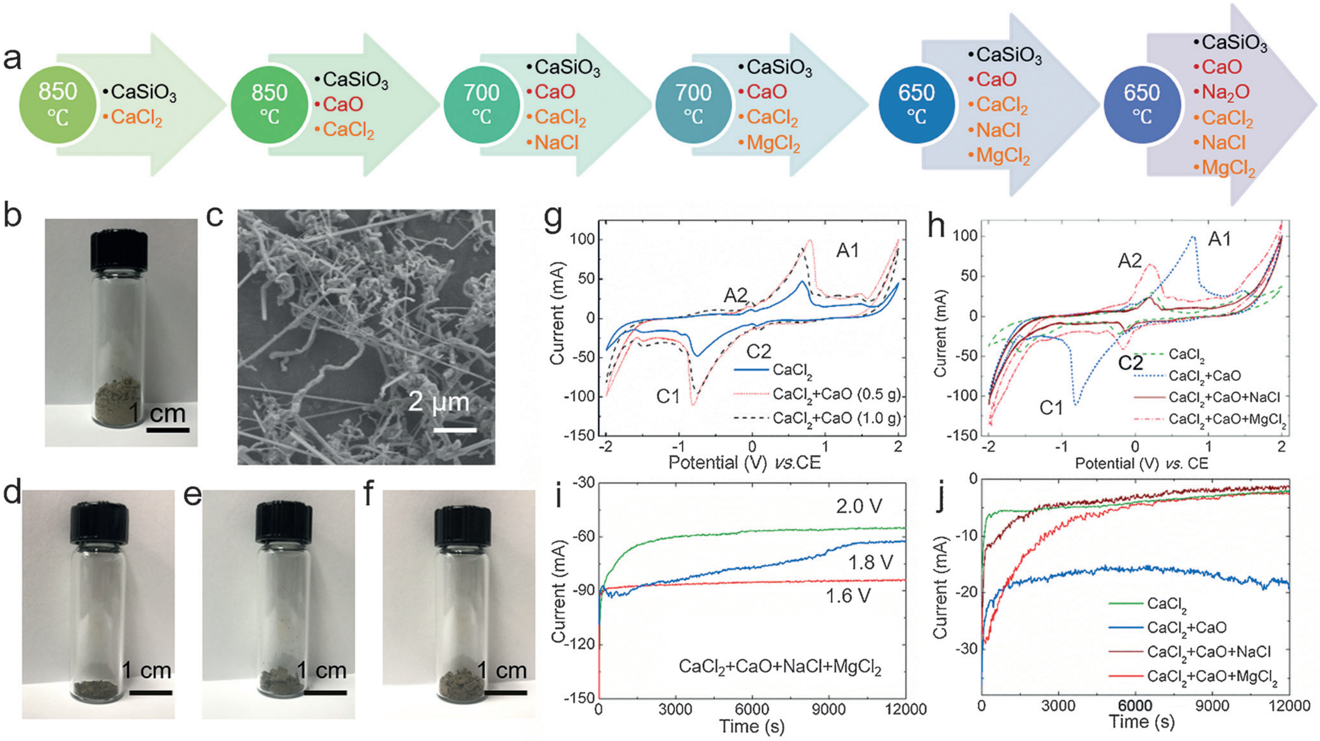

Figure 2. a) The progression of reaction designs that led to the final efficient low-temperature electrochemical reduction of $CaSiO_3$ precursor. b) The product and c) SEM image of the product dispersed on a Si wafer from the electrolysis of $CaSiO_3$ in $CaCl_2$ melt with CaO as supporting electrolyte. d–f) Photographs of the products formed from electrolysis in $CaCl_2$–NaCl, $CaCl_2$–$MgCl_2$, and $CaCl_2$–NaCl–$MgCl_2$ melts. CV curves before the electrochemical reduction process g) with different amounts of CaO added to molten $CaCl_2$ and h) in $CaCl_2$, $CaCl_2$–NaCl, and $CaCl_2$–$MgCl_2$ melts. i) Current–time curves of electrolysis in the optimized $CaCl_2$–NaCl–$MgCl_2$ melts (2:4:1) at constant voltages of −1.6, −1.8, and −2.0 V, j) Current–time curves of electrolysis in $CaCl_2$–NaCl, $CaCl_2$–$MgCl_2$, and $CaCl_2$–NaCl–$MgCl_2$ melts at a constant voltage of −1.6 V.

sized that the product yield is correlated with the solubility of $CaSiO_3$ in the molten salts. Thus, we carried out solubility tests in $CaCl_2$–NaCl and $CaCl_2$–$MgCl_2$. The solubility of $CaSiO_3$ reaches up to 0.8 wt% at 700 °C in $CaCl_2$–$MgCl_2$ mixture, however, it remains marginal (below 0.2 wt%) in $CaCl_2$–NaCl (Supporting Information, Figure S6). We concluded that even though NaCl can lower the melting point, the solubility of $CaSiO_3$ in $CaCl_2$–NaCl is too low to realize low-temperature electrolysis.

To achieve both low melting point and high $CaSiO_3$ solubility to realize low-temperature electrolysis in high yield, we further investigated the ternary eutectic melts of $CaCl_2$–$MgCl_2$–NaCl. A previous report[18] has shown that different salt ratios vary the chemical potentials, thus creating a molten salt eutectic and lowering the melting point and the viscosity of the mixtures. The electrolyte with a mass ratio for NaCl/$CaCl_2$/$MgCl_2$ of 2:4:1 is decreased to 424 °C according to the phase diagram in the Supporting Information, Figure S7. The solubility of $CaSiO_3$ in this melt (Supporting Information, Figure S6) increases with temperature between 450 to 750 °C, but the solubility remains low (less than 0.2 wt%) below 550 °C. However, the solubility increases sharply between 550 and 650 °C to about 1.0 wt% and then further rises to 1.2 wt% at 750 °C. Therefore, we chose a reaction temperature of 650 °C, which is lower than that of the binary melts yet maintains sufficient $CaSiO_3$ solubility, to allow for a fast electrolysis rate and a good yield. As summarized in Table S1, the electrolysis in the most optimized $CaCl_2$–NaCl–$MgCl_2$ ternary melt (with mass ratios of 4:2:1) at 650 °C leads to a Si yield of 75 mg (Figure 2 f), the highest yield among those low-temperature electrolysis reactions. The Coulombic efficiency of electrolysis (electrolytic reaction yield) is generally about 70% for optimized reaction conditions (see the Supporting Information). We further investigated the reaction mechanisms using the different melts under different reaction times and voltages using electrochemical characterization. As shown in Figure 2 h–j and discussed in the Supporting Information, the optimized applied voltage of −1.6 V in the optimized $CaCl_2$–NaCl–$MgCl_2$ melts with the CaO supporting electrolyte at 650 °C indeed show favorable kinetics and stable electrodeposition of Si (Figure 2 i).

The Si produced on the graphite cathode was then separated from the solidified molten salts, cleaned, and characterized. The PXRD patterns of the samples produced under −1.6, −1.8, and −2.0 V (Figure 3 a) were almost identical and could be indexed to Si (JCPDS: 00-027-1402). The sharp diffraction peaks indicated the high crystallinity of the products, and their high purity (99.52%) was confirmed by EDS (Supporting Information, Figure S9) and ICP-AES (Supporting Information, Figure S10). The products from other reactions in different electrolytes were also well-crystallized Si (Supporting Information, Figure S11). SEM images revealed nanowire (NW) morphology for the products

© 2017 Wiley-VCH Verlag GmbH & Co. KGaA, Weinheim

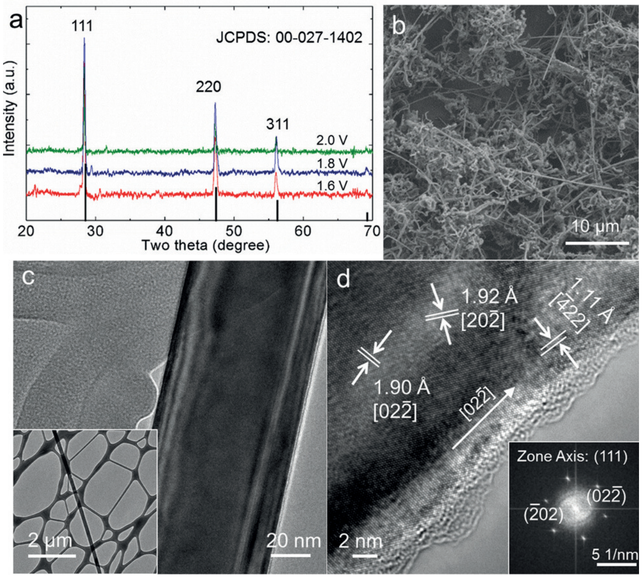

Figure 3. a) XRD patterns of the Si NWs synthesized by using the optimized melts at different voltages in comparison with the standard pattern (JCPDS 00-027-1402). b) SEM, c) TEM, and d) HRTEM images and the corresponding FFT (inset) of the Si NWs produced under the optimized conditions.

made under optimized conditions (Figure 3b) and other conditions (Supporting Information, Figure S12). The NW diameter can be from about 80 to 300 nm and the length is from several up to a hundred micrometers. EDS analysis (Supporting Information, Figure S13) confirmed that the NWs consisted mainly of Si. The oxygen was likely from the formation of a thin native oxide layer. The HRTEM image (Figure 3d) highlights the single crystalline nature of the Si NWs. The cubic Si structure was confirmed by indexing the FFT (Figure 3d). The observed plane spacings of 0.190 and 0.111 nm correspond well to the $(02\bar{2})$ and (422) lattice planes of Si, respectively. The indexed reciprocal lattices show that the NW axes are parallel to the (011) crystal directions. The curved NWs in the SEM image consist of multiple domains assembled together with rough surfaces (Supporting Information, Figure S14). Notably, the reduced Si products are mostly of the NW morphology. This is not fully understood at present but is suspected to be due to metal impurities that could act as catalytic sites essential for the continuous anisotropic growth of Si.[15]

Pure $CaSiO_3$ is not the only soluble Si precursor. For example, common glass is primarily composed of SiO_2, CaO, and Na_2O, and therefore, recycled glass can potentially replace $CaSiO_3$ in this reaction. Therefore, we carried out electrolysis reactions with the addition of Na_2O under the same reaction temperature of 650 °C to explore this possibility (the compositions of different salts and the reaction conditions are summarized in Table S1). As shown in the Supporting Information, Figure S15, the morphology of the product was Si NWs, and PXRD confirmed that the phase was also mainly Si although some impurities were present. In fact, soluble Na_2O could also provide O^{2-} ions in the molten salts just as CaO does; therefore, replacing up to about 40 wt % of CaO with Na_2O in the melt mixture did not seem to affect the reactions. The highest product yield was 80 mg when an optimal combination of 0.40 g CaO and 0.11 g Na_2O was used, which is even slightly higher than the yield from the optimized molten salt mixtures using just CaO. These results, even though not fully optimized, suggest the feasibility for recycling glass waste, or even coal ash (whose major components are also SiO_2 and CaO[19]), to produce value-added Si nanomaterials.

The low temperature electrochemical production of Si in high yield is enabled by three key advances: 1) The use of the soluble $CaSiO_3$ as a precursor to enable the bulk production of Si, 2) the enhanced diffusion of O^{2-} ions resulting from the introduction of the CaO (or Na_2O) supporting electrolyte, and 3) the design of the low melting point ternary $CaCl_2$–NaCl–$MgCl_2$ eutectic molten salts that retain sufficiently high solubility of the $CaSiO_3$ precursor. If a steady-state concentration of CaO in the molten salts is maintained as the reaction proceeds, SiO_2 can also be dissolved into the melts through the formation of $CaSiO_3$ and thus be used directly as a precursor. This successful electrolytic synthesis of Si from the abundant and inexpensive $CaSiO_3$ precursor at 650 °C is more sustainable and practically significant for several reasons. First, the low reaction temperature enables the recycling of residual medium-grade waste heat energy in various industrial and energy technologies and thus improve the overall cycle and power plant efficiencies.[14] Second, metal halide molten salts in the temperature range of 600–700 °C have been successfully utilized in the molten salt nuclear reactors and concentrated solar thermal energy conversion technologies as a heat exchange medium.[13,20] The material compatibility and other practical issues have already been addressed at the industrial scale. Furthermore, this suggests a sustainable pathway to recycle glass waste or coal ash to produce value-added Si nanomaterials.

Electrolytically produced Si NWs are useful materials for high-capacity (ca. 4200 $mAh\,g^{-1}$) Li battery anodes. Nanostructured Si materials, such as Si NWs, can better accommodate the volume expansion involved in the Li battery cycling than bulk Si.[21,22] The charge–discharge profiles of Si NWs at current densities from C/40 to 1C over a potential window of 0.01 to 2.0 V for the first cycle are presented in Figure 4a. The specific discharge capacity at C/40 was 3333 $mAh\,g^{-1}$, indicating that the final structure contains between 2.93 and 3.48 Li atoms per Si atom. The discharge curve exhibited an obvious voltage plateau consistent with previous studies, corresponding to Si alloying with Li.[21] There was an obvious drop in the capacity during the 2nd cycle to 2468 $mAh\,g^{-1}$, which is mainly attributed to the formation of the solid electrolyte interface (SEI) and other side reactions. For the cycling performance under the C/2 rate (Figure 4b), the initial discharge capacity was 2865 $mAh\,g^{-1}$. After 500 cycles, the discharge capacity still reached 714 $mAh\,g^{-1}$. At 1C, the capacity still reached 521 $mAh\,g^{-1}$ (Figure 4c). When the current density returned to C/40, no obvious capacity decay was observed. These results demonstrated the good performance and the promise of these electrochemically synthesized Si NWs as high-capacity Li-ion battery anode materials. Their performance can be further improved by further accommodating the volume change and stabilizing the SEI layer.[22]

© 2017 Wiley-VCH Verlag GmbH & Co. KGaA, Weinheim

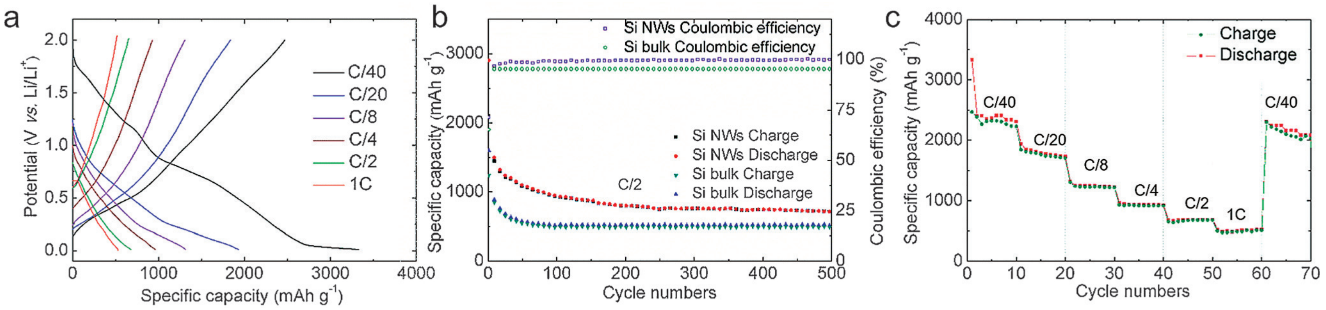

Figure 4. The electrochemical performance of the electrochemically synthesized Si NWs as lithium-ion battery anode material. a) Charge–discharge curves of the Li/Si battery in the potential range of 0.01–2.0 V vs. Li/Li$^+$. b) The cycling performance and the columbic efficiency at a current density C/2. c) The rate performance at the different current density of C/40, C/20, C/8, C/4, C/2, and 1C.

In conclusion, we have developed a novel molten salt electrolysis method to produce Si NWs from an inexpensive soluble $CaSiO_3$ precursor at a low temperature of 650 °C by designing a ternary molten salt system and introducing CaO to facilitate transport of the oxygen ions. These advances enable the electrochemical reduction at 650 °C for effective Si production in high yield. This work opens up a new route for practical and sustainable direct production of Si at an industrial scale that is compatible with existing industrial processes and can be integrated with medium waste heat recycling. It also provides new insights into molten salt electrolysis, which could help to improve other important electrolytic metal extraction processes[8] and introduces the possibility of recycling glass waste and coal ash to produce value-added materials in an environmentally friendly way.

Acknowledgements

This work was supported by a UW-Madison SIRE-REU grant and by the State Key Laboratory of Advanced Technology for Materials and Processing at Wuhan University of Technology (2017-KF-3). Y.D. thanks support from the China Scholarship Council. M.J.S. thanks NSF Graduate Research Fellowship for support. S.N.G acknowledges the support from the NSF SEES Fellowship (EEC-1313968). L.M. thanks the National Natural Science Foundation of China (51521001) and NSFC Distinguished Young Scholars (51425204) for support.

Conflict of interest

The authors declare no conflict of interest.

Keywords: electrolysis · Li-ion batteries · molten salts · silicon nanowires · supporting electrolytes

How to cite: *Angew. Chem. Int. Ed.* **2017**, *56*, 14453–14457
Angew. Chem. **2017**, *129*, 14645–14649

[1] F. Priolo, T. Gregorkiewicz, M. Galli, T. F. Krauss, *Nat. Nanotechnol.* **2014**, *9*, 19.
[2] D. Yue, F. You, S. B. Darling, *Solar Energy* **2014**, *105*, 669.
[3] N. N. Greenwood, A. Earnshaw, *Chemistry of the Elements*, Butterworth-Heinemann, **1997**.
[4] W. Xiao, X. Jin, Y. Deng, D. Wang, G. Z. Chen, *J. Electroanal. Chem.* **2010**, *639*, 130.
[5] H. Yin, X. Mao, D. Tang, W. Xiao, L. Xing, H. Zhu, D. Wang, D. R. Sadoway, *Energy Environ. Sci.* **2013**, *6*, 1538.
[6] K. Yasuda, K. Morita, T. H. Okabe, *Energy Technol.* **2014**, *2*, 141.
[7] A. Bao, M. R. Weatherspoon, S. Shian, Y. Cai, P. D. Graham, S. M. Allan, G. Ahmad, M. B. Dickerson, B. C. Church, Z. Kang, H. W. Abernathy, C. J. Summers, M. Liu, K. H. Sandhage, *Nature* **2007**, *446*, 172; B. Luo, X. Wang, C. Meyers, N. Wannenmacher, W. Sirisaksoontorn, M. M. Lerner, X. Ji, *Sci. Rep.* **2013**, *3*, 2222.
[8] G. Z. Chen, D. J. Fray, T. W. Farthing, *Nature* **2000**, *407*, 361; C. A. M. Abdelkader, K. T. Kilby, A. Cox, D. J. Fray, *Chem. Rev.* **2013**, *113*, 2863.
[9] A. Nohira, K. Yasuda, Y. Ito, *Nat. Mater.* **2003**, *2*, 397; B. X. Jin, P. Gao, D. Wang, X. Hu, G. Z. Chen, *Angew. Chem. Int. Ed.* **2004**, *43*, 733; *Angew. Chem.* **2004**, *116*, 751.
[10] H. Yin, B. Chung, D. R. Sadoway, *Nat. Commun.* **2016**, *7*, 12584; A. Allanore, L. Yin, D. R. Sadoway, *Nature* **2013**, *497*, 353.
[11] D. Wang, X. Jin, G. Z. Chen, *Annu. Rep. Phys. Chem.* **2008**, *104*, 189.
[12] W. Xiao, X. Wang, H. Yin, H. Zhu, X. Mao, D. Wang, *RSC Adv.* **2012**, *2*, 7588.
[13] R. K. Shah, D. P. Sekulic, *Fundamentals of Heat Exchanger Design*, Wiley, New York, **2003**.
[14] W. A. Phillip, *Nat. Energy* **2016**, *1*, 16101.
[15] W. Xiao, J. Zhou, L. Yu, D. Wang, X. W. D. Lou, *Angew. Chem. Int. Ed.* **2016**, *55*, 7427; *Angew. Chem.* **2016**, *128*, 7553; B. S. K. Cho, F.-R. F. Fan, A. J. Bard, *Angew. Chem. Int. Ed.* **2012**, *51*, 12740; *Angew. Chem.* **2012**, *124*, 12912.
[16] W. Xiao, D. Wang, *Chem. Soc. Rev.* **2014**, *43*, 3215.
[17] S. Wang, F. Zhang, X. Liu, L. Zhang, *Thermochim. Acta* **2008**, *470*, 105.
[18] T. Østvold, *Acta Chem. Scand.* **1972**, *26*, 1751.
[19] S. K. Ritter, *Chem. Eng. News* **2016**, *94*, 10.
[20] J. Serp, M. Allibert, O. Beneš, S. Delpech, O. Feynberg, V. Ghetta, D. Heuer, D. Holcomb, V. Ignatiev, J. L. Kloosterman, L. Luzzi, E. Merle-Lucotte, J. Uhlíř, R. Yoshioka, D. Zhimin, *Prog. Nucl. Energy* **2014**, *77*, 308.
[21] S. W. Lee, H.-W. Lee, I. Ryu, W. D. Nix, H. Gao, Y. Cui, *Nat. Commun.* **2015**, *6*, 7533.
[22] N. Liu, Z. Lu, J. Zhao, M. T. McDowell, H. Lee, W. Zhao, Y. Cui, *Nat. Nanotechnol.* **2014**, *9*, 187; J. R. Szczech, S. Jin, *Energy Environ. Sci.*, **2011**, *4*, 56.

Manuscript received: July 18, 2017
Revised manuscript received: August 23, 2017
Accepted manuscript online: September 26, 2017
Version of record online: October 18, 2017

© 2017 Wiley-VCH Verlag GmbH & Co. KGaA, Weinheim